Mutual interactions between plasma filaments in a tokamak evidenced by fast imaging and machine learning

Sarah Chouchene, Frédéric Brochard, Nicolas Lemoine, Jordan Cavalier, Mikael Desecures, Vladimir Weinzettl

Mutual interactions between plasma filaments in a tokamak evidenced by fast imaging and machine learning

Sarah Chouchene,[1,2,*] Frédéric Brochard,[1,†] Nicolas Lemoine,[1,‡]
Jordan Cavalier,[3,§] Mikael Desecures,[2,¶] and Vladimir Weinzettl[3,**]

[1] *Université de Lorraine,Institut Jean Lamour, CNRS, Nancy, 54000, France*
[2] *APREX Solutions, Pulligny 54160, France*
[3] *Institute of Plasma Physics of the CAS, Prague 8, 18200, Czech Republic*

(Dated: April 4, 2024)

Magnetically confined fusion plasmas are subject to various instabilities that cause turbulent transport of particles and heat across the magnetic field. In the edge plasma region, this transport takes the form of long filaments stretched along the magnetic field lines. Understanding the dynamics of these filaments, referred to as blobs, is crucial for predicting and controlling their impact on reactor performance. To achieve this, highly-resolved passive fast camera measurements have been conducted on the COMPASS tokamak. These measurements are analyzed using both conventional tracking methods and a custom-developed machine learning approach designed to characterize more particularly the mutual interactions between filaments. Our findings demonstrate that up to 18% of blobs exhibit mutual interactions in the investigated area close to the separatrix, at the border between confined and non-confined plasma. Notably, we present direct observations and radial dependence of blob coalescence and splitting, as well as rapid reversals in the blob's propagation direction, as well as their dependence on the radial position. The comparison between observations realized with passive imaging and Gas Puff Imaging does not evidence any significant bias due to the use of the latter technique.

Keywords: Turbulent transport, Plasma filament, Machine learning, Magnetic confinement, High-temperature plasma, Tokamak

I. INTRODUCTION

Nuclear fusion holds the promise of providing an almost limitless source of clean energy. While the potential role of fusion in the energy transition is debated, industrially worldwide important countries have included fusion as one of the proposed solutions with the highest potential [1]. Despite significant progresses have been made, with important milestones achieved in recent years [2–6], the ability to generate electricity from nuclear fusion on a large scale and within a reasonable time frame is still unclear. Currently, the most promising device for producing electricity by nuclear fusion is the tokamak, a type of fusion reactor that utilizes nested magnetic surfaces to confine and stabilize a high-temperature plasma. Several such devices are in operation or under development in the world, including the ITER project [7], which aims to demonstrate the feasibility of large-scale nuclear fusion power generation. However, even with the latest technological and scientific advances, the production of electricity through nuclear fusion remains a formidable task. The emergence of private companies promising the first fusion power plants in the coming decade [8] should not overshadow that numerous challenges persist in crucial areas such as plasma confinement, plasma heating, materials and tritium fuel cycle [9].

Magnetically confined plasma are susceptible to various instabilities that contribute to turbulent transport through the magnetic surfaces [10]. The losses of particles and heat resulting from this transport across the magnetic field have been a challenging research topic for decades. One key phenomenon involved in this transport is the formation and propagation of plasma filaments, referred to as blobs [11–14]. Blobs are coherent structures elongated along the magnetic field lines, propagating radially outward in the edge region of tokamaks. They can induce mixing between the core and edge plasma, leading to energy and particle transport across the magnetic field lines. In addition to energy losses, blobs can also contribute to wall erosion and to the injection of impurities from the wall into the confined region, posing significant challenges that need to be addressed to enhance device performance and longevity [10].

Experimental studies utilizing different plasma diagnostic methods have shown that blobs cross-sections in the poloidal plane have a diameter ranging from a few millimeters to a few centimeters and a characteristic lifetime of the order of 10 µs [15]. Achieving the necessary spatial and temporal resolutions to adequately resolve blob dynamics with cameras often relies on a technique called gas puff imaging (GPI), which involves the localized injection of gas at the camera's focal plane to improve the signal-to-noise ratio (SNR) and enhance structure localization [16]. Such measurements have demonstrated that blobs are often expelled from the Last Closed Flux Surface (LCFS) region [17]. In order to study the

* sarah.chouchene@univ-lorraine.fr
† frederic.brochard@univ-lorraine.fr
‡ nicolas.lemoine@univ-lorraine.fr
§ cavalier@ipp.cas.cz
¶ mikael.desecures@aprex-solutions.com
** weinzettl@ipp.cas.cz

rapid dynamics of filaments, various imaging techniques have been developed since the early 2000s. Temporal resolutions of 1µs were achieved as early as 2003 on Alcator C-mod and NSTX tokamaks by using GPI, but with cameras that could only record short sequences (typically six consecutive images), or temporally uncorrelated snapshots [18–20]. In 2010, long sequences with an unprecedented temporal resolution of 500 ns were achieved on Alcator C-mod [21], and more recently on the TCV tokamak [15] still with GPI, enabling to resolve individual blob dynamics and to conduct statistically robust investigations. At the COMPASS tokamak [22], the recycling of neutrals at the wall can provide sufficient visible light to investigate the dynamics of blobs without the necessity of additional gas injection, on condition to use a tomographic inversion method for their localization [23, 24]. Although measurements obtained with this approach have a less favorable SNR compared to GPI measurements, they offer the advantage of being completely non-perturbative, while disturbances induced by GPI are challenging to evaluate [16].

The results presented in this paper are based on measurements obtained during the last operational campaign of the COMPASS tokamak before its final shutdown, where passive fast imaging data with frame rates up to 1.008 million frames per second have been obtained in L-mode discharges. These high-speed recordings reveal dynamical behaviors that could only be speculated upon with recordings made at lower rates. Our observations unequivocally show that the poloidal velocity of blobs at a given point frequently reverses, regardless of their radial location in the vicinity of the LCFS. This feature may pose significant tracking challenges in videos recorded at lower frame rates, as we explain in section III- Data analysis and results. Furthermore, our observations reveal that blobs interact with each other, exhibiting phenomena such as coalescence and splitting. Previous theoretical works and simulations have debated whether interactions occur between blobs. Some simulations, starting with isolated blobs, suggest little to no interaction [25], while others, where blobs exist within a consistent turbulent plasma background, suggest that almost half of them interact with each other [26].

Experimentally the large waiting time between events identified as blobs in probe data at a single point in the Scrape-Off-Layer (SOL) has long been used to argue in favor of independence between filaments and low probability of mutual interactions between filaments [27–29], until experimental evidence of this type of interactions was provided by GPI recordings on several tokamaks. The possibility of blob collisions, merging or splitting is thus taken into account in several analysis tools set up to study ELMs or blob dynamics, e.g. on NSTX [30, 31] or TCV [32, 33]. However, the experimental studies published to date did not focus on the study of these interactions, and the methods used are not necessarily able to provide statistically significant data. For instance, the frequency of these events is generally not discussed, and even if Offeddu et al. estimate the splitting frequency at 10% and the merging frequency at 3%, the total number of filaments considered, 154, is certainly too low to draw firm conclusions [32]. In contrast to these work, the method we have developed and which is presented in this study is specifically designed to target this type of interactions and enable their statistical study in large datasets. For example, on shot #20846 alone, for which the video recording corresponds to 50 ms of discharge, our method counts 6025 filaments, 18% of which are interacting. As the analysis is fully automated (after the model has been properly trained), our method makes it easy to analyze a large number of videos, and confers real statistical value to the study of filament interactions.

In order to automate the detection of interaction phenomena between blobs, we have opted for a machine learning (ML) approach. ML methods and particularly convolutional neural networks (CNNs) have proven to be highly effective in computer vision and image recognition tasks, and have been successfully applied in quantum physics [34], nuclear physics [35], human sciences [36], medicine [37] and many other domains [38, 39]. In plasmas physics, such techniques have been recently used to detect and track blobs in 2D videos [15], an approach different to the one that we present in this paper, which is based on the application of YoloV7-segmentation [40] to time-integrated pictures, as explained in section III. More specialized approaches using Deep-Learning (DL) have also been used to recover the plasma dynamics from partial observations [41] and recently to quantify interaction forces such as electric field between blobs on turbulent scale [42].

II. EXPERIMENTAL SETUP

Our investigations are based on tomographically inverted data captured by a single fast visible camera observing the edge plasma region in L-mode D-shaped discharges, considering constant light emissivity along the magnetic field lines [24]. This approach produces 2D maps of light fluctuations in a poloidal plane, in a 10 cm square located on both sides of the LCFS, with a pixel (node) resolution of 2 mm. We primarily focus on the COMPASS discharge #20846, which has been captured at a high frame rate of 1,008 million frames per second (fps) and an exposure time of 0.68 µs. The high spatial and temporal resolutions enable to resolve the turbulence dynamics and to evidence mutual interactions between blobs, but the presence of an intermittent gas puff source in the camera field of view might perturb the dynamics and questions the validity of the tomographic inversion. To investigate theses issues, two other shots, recorded at 900 kfps are analyzed, one involving a stable gas puff injection during the video acquisition (discharge #20849) and another one completely without gas puff during the acquisition (discharge #20987). A sketch presenting the experimental setup is given in Fig.1.

Table I provides a summary of the most important parameters used in this study.

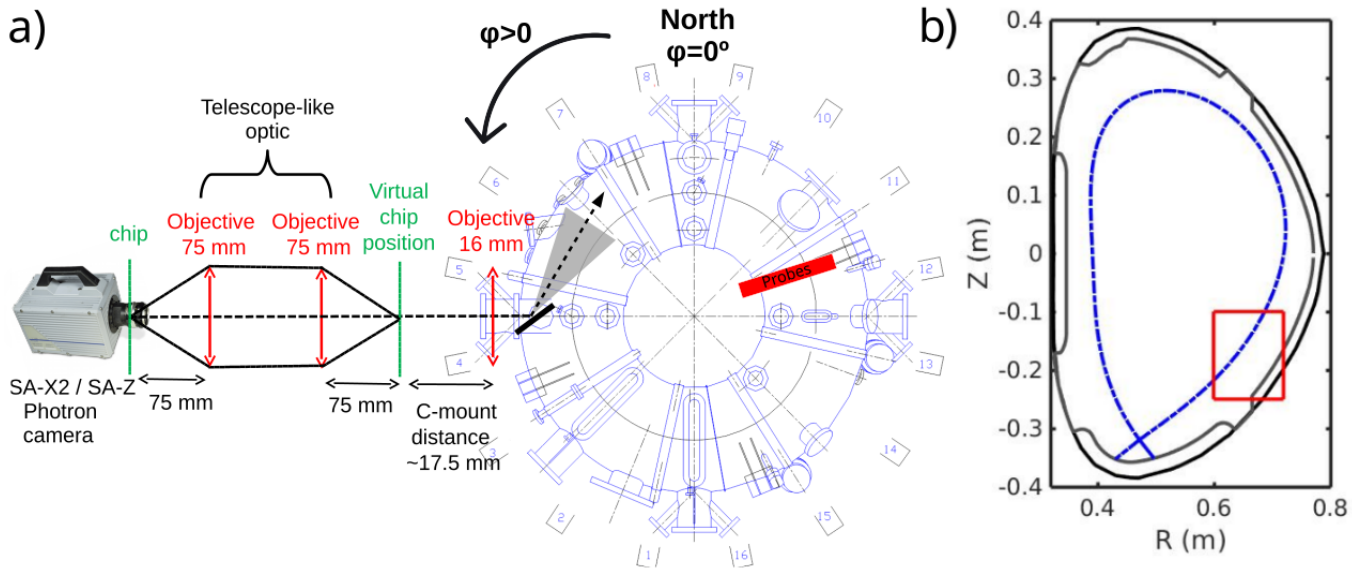

FIG. 1: **a)** Schematic of the optical setup installed on COMPASS (top view). **b)** Poloidal cross-section of the camera field of view. [24].

TABLE I: Main parameters of the shots investigated in our study

Shots	Frame rate (kfps)	Exposure time (µs)	Toroidal magnetic field B_T (Tesla)	Plasma current $I_p(kA)$	Flat-top plasma density n_e $(10^{19}m^{-3})$	Camera window Width x Height (pixels)
20846	1008	0.68	-1.15	182	4	128 x 40
20849	900	0.79	-1.5	383	3	128 x 56
20987	900	0.79	-1.38	-271	6	128 x 56

III. DATA ANALYSIS AND RESULTS

A. Highly resolved conventional analysis

Inverted camera data are first analyzed using the AX R&D software [43] in order to detect and track turbulent structures individually. This analysis is carried out with conventional thresholding techniques for blob contouring and a bayesian approach for their tracking. Fig. 2 depicts the 2D map of the temporally averaged poloidal blob velocities thus reconstructed for shot #20846. The core plasma is located on the left side of the LCFS, while the right side represents the SOL. The mean poloidal velocities map exhibits a shear zone radially distant between 2 mm to 4 mm outside the LCFS. The LCFS position itself is obtained by the EFIT reconstruction, which has a precision of about 1 cm, as checked by probe measurements [44]. The time-averaged probability density functions (PDFs) of poloidal velocities in a 4 mm square are depicted in Fig. 3(a), as well as the time series of poloidal velocities in the same zone (Fig. 3(b)).

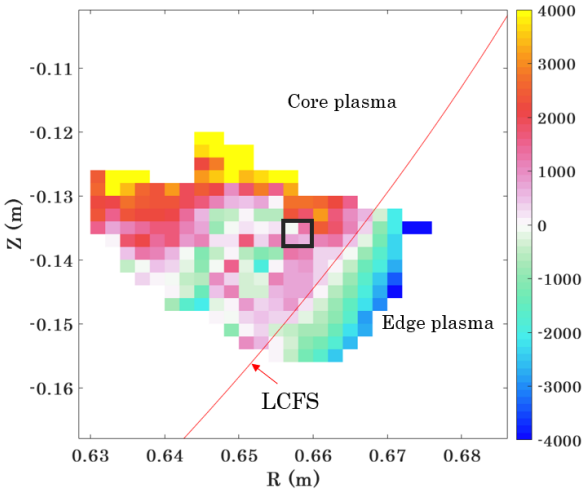

FIG. 2: 2D map of the mean poloidal velocities per pixel (m/s) of shot 20846 at [1100 - 1146.6] ms; The black square is the selected area. [color online]

This figure shows that while time-averaged velocity maps offer a comprehensible and apparently satisfactory picture of flows in the vicinity of the LCFS, they do not capture the true complexity of blob dynamics as already illustrated in [32, 45] for instance. Indeed, Fig. 3 reveal that average (or most probable) velocities only imperfectly account for the movement of blobs, whose direction frequently reverses, even relatively far from the shear zone. These fast reversals of the propagation direction are observed whatever the location of the area selected in the 2D map and are common to all our analyses, whatever the discharge conditions. The manual analysis of different sequences confirms that these are not tracking errors, which are likely to occur if the frame rate is too low. Such fast reversal is illustrated in Fig. 4, where a sequence showing downstream filament motion (Fig. 4(a)) is shortly followed by upstream motion in the poloidal direction (Fig. 4(b)). Some sequences show that the speed reversal sometimes takes only a few microseconds, with the same blob reversing its movement, ordinary in the presence of another blob, suggesting possible mutual interactions. Two other features are not visible, or at least not unequivocally so, at lower acquisition frequencies: the merging or splitting of blobs. Fig. 4(c) illustrates an example of a coalescence interaction sequence where three blobs merge to form a single one, while Fig. 4(d) represents the splitting of one filament into two distinct structures.

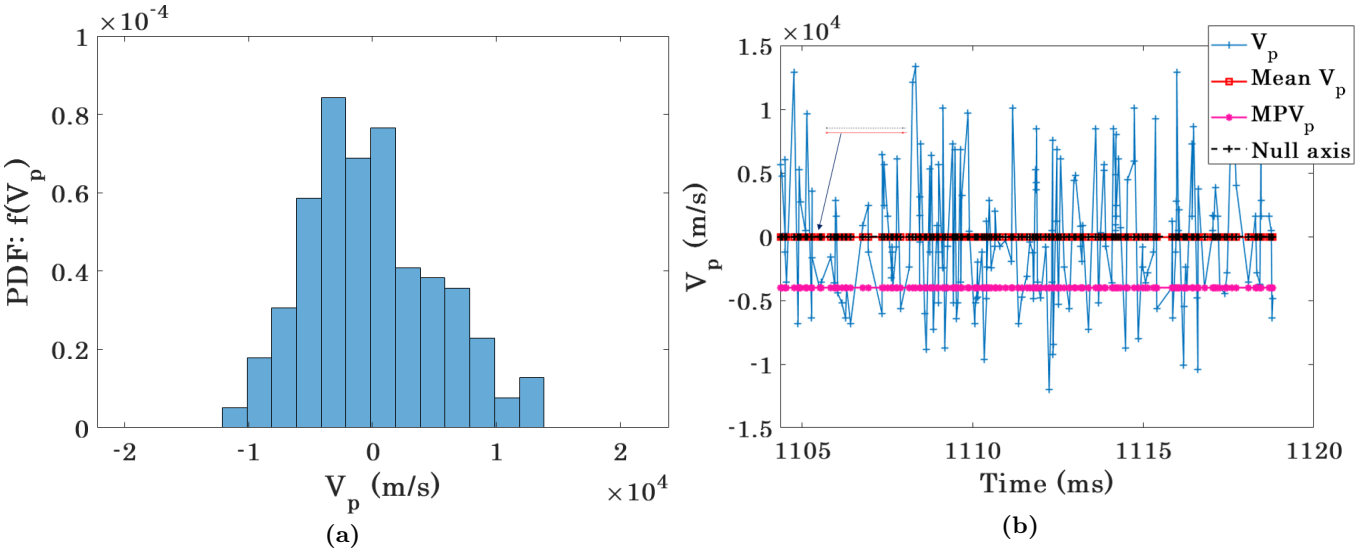

FIG. 3: (a) Probability density function (PDF) of the poloidal velocities V_P of filaments in the area included in the black square depicted in Fig. 1, where the most probable velocity $MPV = -4000$ m/s and the Mean $V_P = -40$ m/s; (b) Temporal variations of poloidal velocities, inside the selected area. In the captions, P stands for poloidal.

B. Poloidal dynamics of filaments

In order to determine whether these dynamical behaviors are statistically significant, it is necessary to automate their detection, which is complex with conventional methods. Restricting ourselves to the poloidal dynamics of blobs, it is however possible to simply visualize them by constructing kymographs, i.e. spatio-temporal representations of the temporal evolution of the light taken along a magnetic flux surface, as shown in Fig. 5 (a), which evidences the poloidal dynamics of blobs over a time interval of 100 µs in the window localized 4 mm radially outside the LCFS depicted in Fig. 5 (b). In such representations, the poloidal propagation direction is immediately inferred from the orientation of the stripes (to the top-right for upstream displacement or to the bottom-right for downstream displacement), while bifurcations are related to either blob coalescence (two stripes merging into a single one as time increases) or blob splitting (one stripe being divided into several ones as time increases). Such patterns can rather easily be extracted with a customized machine learning (ML) approach, as we now explain.

C. Machine Learning characterization and dataset benchmark

To achieve the final detection results using machine learning (ML), data undergoes a two-step process. First, as illustrated in Fig. 6, data is preprocessed as follows: 2D turbulence images of a specific discharge are obtained from the ultrafast camera (Photron SA-Z). The temporal median is subtracted from the raw image to enhance light fluctuations, revealing blobs [46]. A tomographic inversion is then applied [23, 24] after determination of the lines of sights with the Calcam software [47]. Additionally, a Bernsen local threshold is used to remove

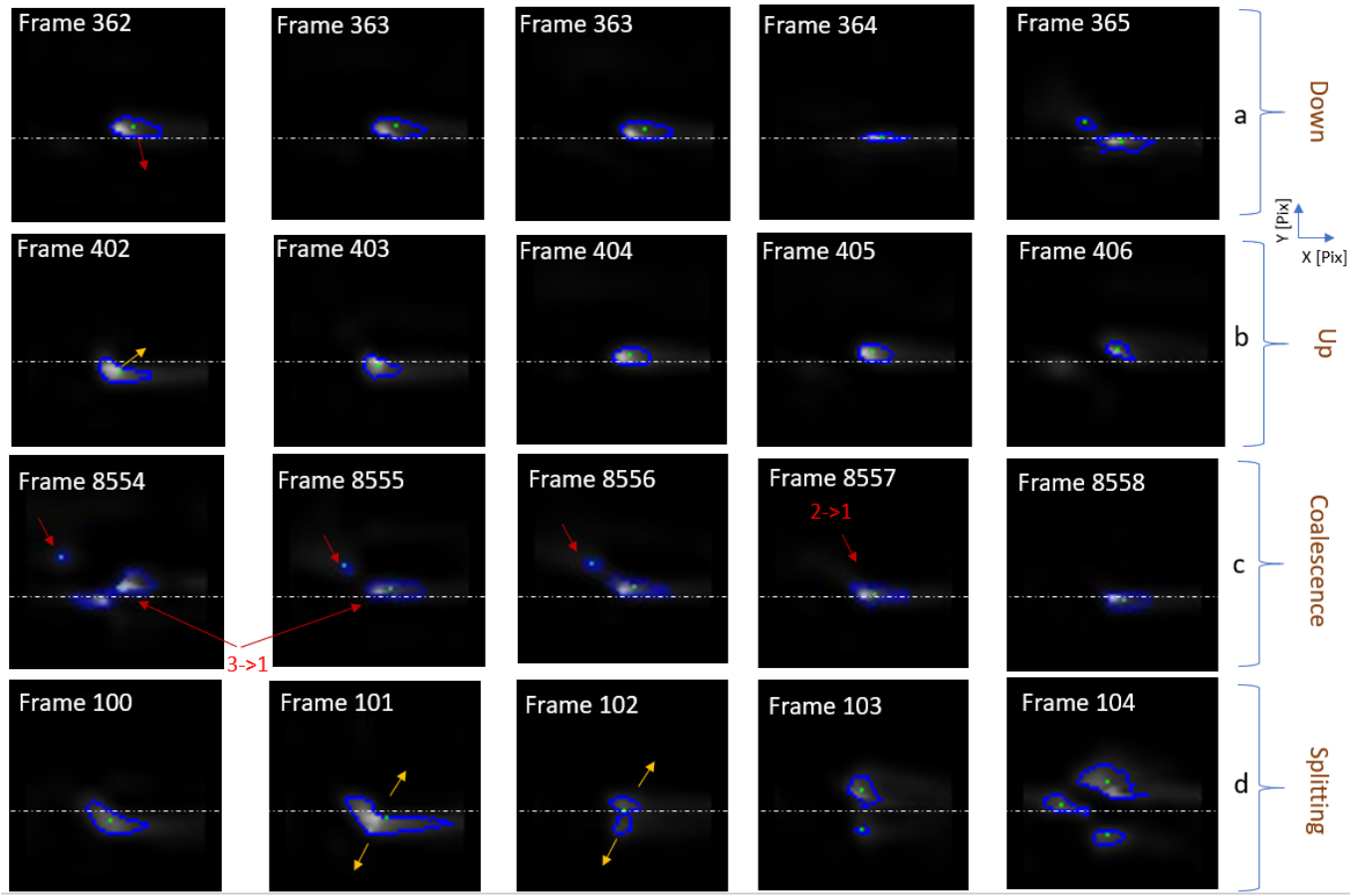

FIG. 4: Downward displacement of filament (a) quickly followed by upward displacement (b), coalescence (c) and splitting (d) observed after tomographic reconstruction in horizontal sequences of successive frames for each phenomena taken each 1 µs in shot #20846. [color online]

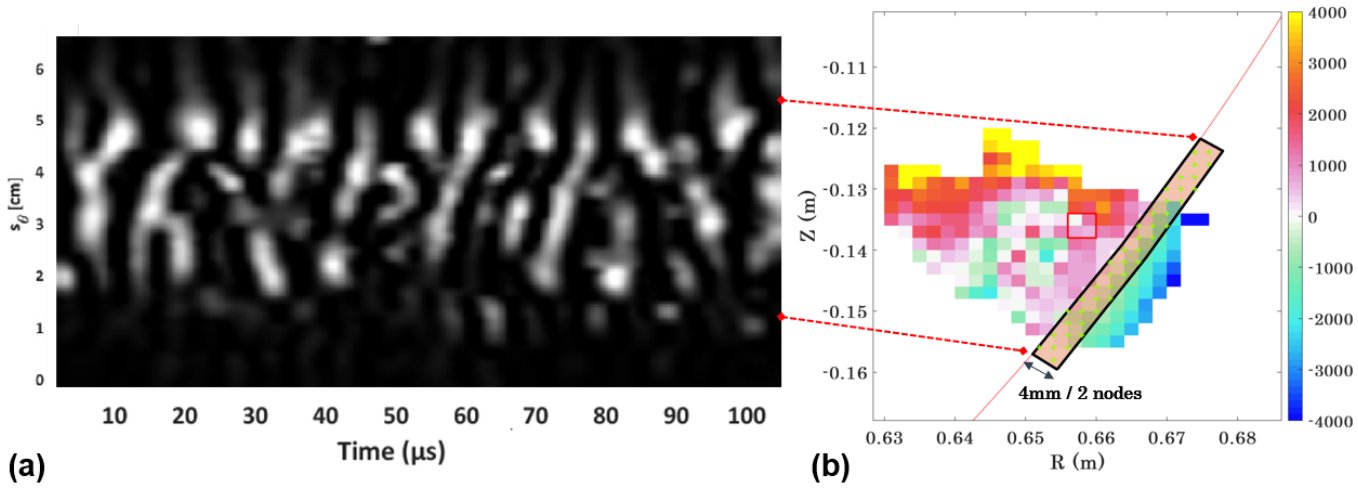

FIG. 5: **(a)** Kymograph showing the time evolution of the image of filaments along a given magnetic flux surface 4 mm outward the LCFS represented as the red (light gray) line, as highlighted in **(b)**. Various behaviors can be observed, such as merging, splitting and fast reversal of the poloidal propagation direction. S_θ is the poloidal curvilinear abcissa. [color online]

reconstruction artifacts. This threshold is based on the local contrast of the image and set to the average of the

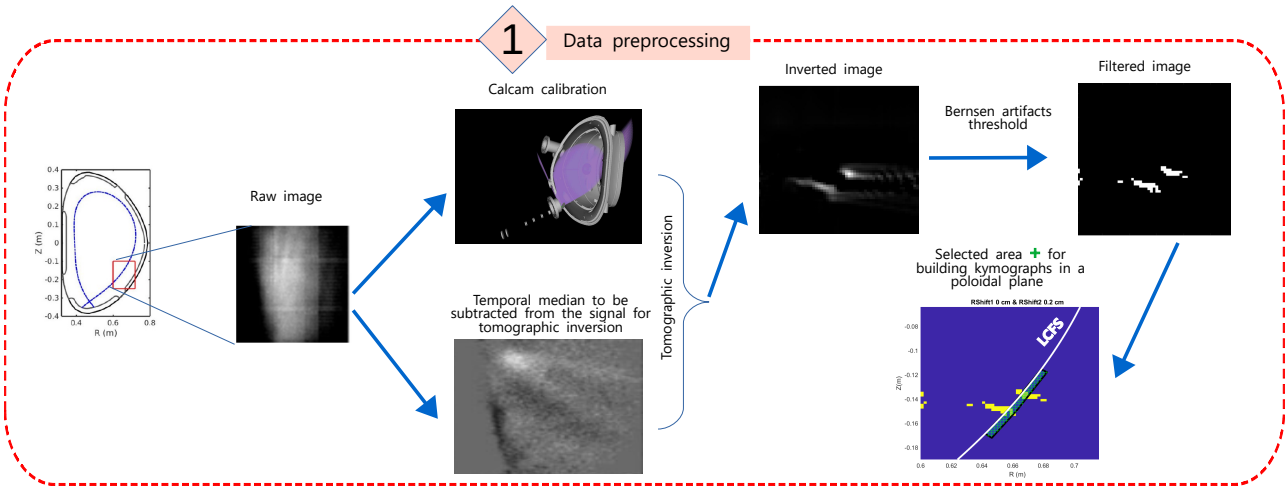

FIG. 6: Overview of the procedure used to generate kymographs. [color online]

maximum and minimum pixel values in the local window. Finally, kymographs are generated from the resulting thresholded images by selecting pixels aligned along constant flux surfaces (corresponding to the selected area "+" in Fig. 5 and Fig. 6), with a time interval of 100 µs, for different distances from the LCFS. Then, object detection deep learning network based on three essential modules is applied, as explained in Appendix A and as summarized in Fig. 8. The ML approach has been set to detect five categories of blob dynamics: *merging*, *splitting*, *up* -for upward motion, *down* -for downward motion, and *reverse* for single blobs reversing their poloidal motion in the observation window. Once trained using 2300 manually annotated kymographs with 13,900 labels of the five filament dynamics categories as input of the customized Yolov7-seg network, it allows for the quantification of filament interactions and displacements near the LCFS without human assistance (Appendix A).

By analyzing kymographs generated along different magnetic flux surfaces, it is possible to investigate the radial dependence of the five categories of blob dynamics. The studied region was therefore divided into 10 equidistant stripes aligned along flux surfaces, and kymographs were generated by averaging the light within 4 mm (2 pixels) in the radial direction. 10 series of 500 kymographs were generated, corresponding to a total time interval of 50 ms during which the EFIT reconstruction shows stable LCFS. The radial profiles of occurrences of the five categories of blob dynamics are displayed in Fig. 7. First, it can be seen that blobs moving upstream or downstream the poloidal direction are met at any radius. More specifically, whereas most blobs move poloidally upward in the confined region (corresponding to negative radial distances relatively to the LCFS), the trend reverses at a distance of about 4 mm towards the wall. This observation is perfectly consistent with the observation of the shear zone depicted in Fig. 2 after conventional 2D tracking analysis. Mutual interactions are also shown to be dominated by splitting processes, whose occurence is relatively constant within the range of radii investigated, while merging processes are mostly detected in the confined region and become more and more negligible after crossing the shear layer. Fast reversals of single blob motion exist whatever the radius, but are unsignificant compared to the other studied phenomena. At both extremities of the radial domain, the total number of detections decreases whatever the category, due to the degraded SNR ratio: indeed, the visible light emission in these region is much lower, resulting in choppy kymographs more difficult to analyze.

Additionally, the slope defined by the aspect ratio of the bounding box surrounding the detected features can be used to calculate automatically a mean poloidal velocity for each blob, and then mean and most probable poloidal velocities profiles at each radius. The accuracy of these velocities was validated by comparing them with the conventional tracking analysis conducted with the AX R&D software. The comparison reveals consistent positions of the shear zone and nearly similar poloidal velocities, except for poloidal velocities lower than 1 km/s, which are never found with the ML approach. Actually, 2D tracking shows that such blobs relatively slow in the poloidal direction have a more significant radial motion, and hence leave only a slight trace on the poloidal kymograph. On the contrary, the ML/kymograph approach is expected to be more efficient in tracking fast blobs than conventional 2D tracking based on predictions made with an insufficient number of frames. All in all, combining both approaches enables to better characterize blob poloidal motion.

The analysis carried out for the other discharges presented in table I yields similar results, indicating that

7% to 18% of blobs experience merging, splitting or quick reversal of the structures' poloidal direction in a close vicinity of the LCFS. This ratio is 11% for discharge #20987, without gas puff, suggesting that there is no blatant bias in our analysis due to the gas puff.

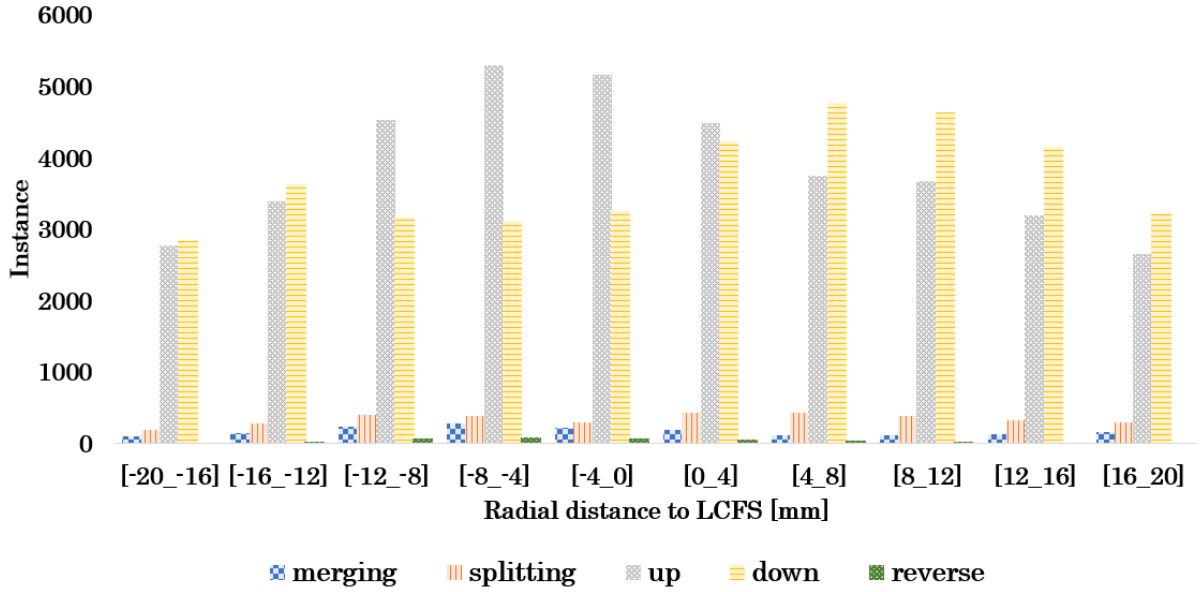

FIG. 7: Instance of detected classes in kymographs generated at different distances from the LCFS, spatially averaged over 4 mm in the radial direction, for discharge #20846. The shear zone is evidenced close to R = +4 mm with respect to the LCFS, where the numbers of structures going up and down almost correspond. [color online]

IV. CONCLUSION

In this work, we have presented a machine learning technique that is well suited to characterizing the complex dynamic behavior of blobs and their mutual interactions. The observation of such interactions first rely on highly resolved fast visible camera measurements, with both high temporal and spatial resolutions. In our earlier measurements recorded at lower frame rates (up to 480 kfps) but with the same spatial resolution [24], mutual blob interactions went unnoticed and tracking results using conventional methods were questionable, as there were doubts about the reality of rapid reversals of blob movement in the poloidal direction, which are indisputable with the improved temporal resolution of 1 µs.

Our observations are consistent with former experimental work which evidenced this type of interactions by using GPI [31, 33] and they support results of simulations with a consistent turbulent background [26], as opposed to seeded blob simulations. The percentage of blobs being involved in mutual interactions, up to 18%, is significant and might be underestimated, given that i) the studied area allowed by the visible light emission is limited to a narrow band close to the LCFS and ii) our method is currently unable to track blobs in adjacent kymographs. This ratio is lower than the value of 50% given in [26] and of the same order as the value of 13% previously found on TCV with a conventional analysis carried out with GPI on a much smaller data set of 154 filaments [32]. The presented ML method has been benchmarked against a state-of-the-art conventional 2D tracking software. Analysis results from 2D tracking show the existence of a large number of counter-propagating structures in both poloidal and radial directions (Appendix B) and are consistent again with similar observations realized with GPI on other tokamaks [32, 33, 45], as well as with simulations results [26]. The ML approach that we have implemented is not suited to the study of radial displacements, but it shows excellent agreement with the tracking results in the poloidal direction. This excellent overall agreement between two approaches, which are based on very different principles and limitations, give us good confidence that our measurements of the poloidal velocity is correct. In our opinion, the evidence of such a large fraction of counter-propagating blobs heavily questions the validity of the tracking results obtained with conventional techniques at lower frame rates. Obviously, the critical temporal resolution to resolve blobs' dynamics depends on the experimental conditions, therefore to reduce errors resulting from insufficient acquisition speed, we recommend comparing the results obtained with manual tracking performed on a few sequences of frames. Alternatively, an automated analysis can be run on downsampled data, for example by removing one image out of two, and comparing the results. In tests carried out on such downsampled data, the filaments' velocities

derived from the ML-kymographs method proved more robust than the conventional tracking method. However the ratio of blobs involved in mutual interactions was found significantly lower than in the original 1 MHz dataset, underlining the importance of achieving such a high frame rate under our experimental conditions. The strong similarities between the observations realized with and without gas puff finally suggest that the blobs interactions are not strongly affected by GPI used to feed the plasma, and that mutual interactions between blobs are inherent to their dynamics in the LCFS region. This means that one of the main drawback of our method, the rather poor SNR at high frame rates, could be overcome by performing GPI measurements which could be considered as non significantly perturbative.

To summarize, the ML method developed for our investigation is clearly complementary to more conventional 2D tracking analysis approaches, and offers several interesting perspectives. It can, for instance, be applied to simulation results in order to improve the cross-comparison with experiments, in the perspective of validating or improving theoretical models. It will be applied to the wide database of COMPASS in order to investigate blobs dynamics under various conditions such as different plasma densities, current and triangularity, L-H transition and the influence of probes on blob's dynamics. By training models on such large datasets, it will become possible to predict and anticipate filament behaviors in various scenarios. This predictive capability can guide experimental design and optimization, reducing the need for exhaustive trial and error. Real-time prediction would be possible in tokamaks using models such as custom Yolov7-segmentation. To interpret the observations presented in this paper, it is necessary to study the physical mechanisms involved in filament interactions. Quantifying the interaction forces between filaments could be achieved by using a physics-informed neural network approach such as the one proposed in [42]. Finally, the application of such ML algorithms to turbulent media paves the way for future researches, enabling not only a better understanding and prediction of blobs dynamics in fusion devices, but also for investigating the interactions between coherent structures in other fields such as fluid mechanics, materials science or low-temperature and dusty plasma, where similar behaviors can be studied [48].

ACKNOWLEDGMENTS

This work was supported by the PLUS project co-funded by FEDER-FSE Lorraine et Massif des Vosges 2014-2020, a European Union Program, and by the french national research agency (Agence Nationale de la Recherche) under project PLATUN ANR-21-CE30-0063, and co-funded by the MEYS project No. LM2023045. This work has been carried out within the framework of the EUROfusion Consortium, funded by the European Union via the Euratom Research and Training Programme (Grant Agreement No 101052200 — EUROfusion). Views and opinions expressed are however those of the authors only and do not necessarily reflect those of the European Union or the European Commission. Neither the European Union nor the European Commission can be held responsible for them. S.C. thanks APREX Solutions and the Region Grand-Est for the funding of her Ph.D. work and all the COMPASS team for carrying out the experiments.

Appendix A: ML method explanation

After the preprocessing step, a machine learning method is applied to the kymographs as explained in Fig. 8. The backbone module, as shown in Fig. 8 (a), is responsible for feature extraction and is based on the efficient layer aggregation networks (ELAN) [49]. It uses a set of convolutional layers to perform feature selection and dimensionality reduction. The extended efficient layer aggregation networks (E-ELAN) is developed and used as the core of the Yolov7 architecture, incorporating an attention mechanism to the layer aggregation module to improve information on the dimensionality of feature extraction channels [50]. The neck module, depicted in Fig. 8 (b), fuses features from different levels of the backbone network to improve detection accuracy. It employs feature pyramid networks (FPN) [51], which address the issue of scale variation in object detection and image segmentation tasks. FPN creates a feature pyramid consisting of feature maps at multiple scales, combining feature maps from higher and lower levels of the network hierarchy. This improves the accuracy of detection and segmentation tasks, especially for objects appearing at different scales. Path Aggregation Network (PAN) [52] is also used to assign a class label to each pixel in an image. It is designed for semantic segmentation tasks, and combines fine-grained and coarse-grained features using a path aggregation module. Finally, the head module, as shown in Fig. 6 (c), predicts bounding boxes and class probabilities for each anchor. It utilizes YOLOR base [53] and includes a segmentation head for class label prediction and a fully-connected (FC) layer for generating a one-dimensional vector representing the flattened feature maps. The outputs are divided into classification probabilities and bounding box coordinates for each object in the image. Region of interest (ROI) pooling is employed to extract small feature maps for object detection or segmentation tasks. Non-maximum suppression (NMS) [54] is applied as a post-processing technique to remove redundant and overlapping detections, selecting the most likely detection based on confidence scores. As an example, Fig. 9 illustrates the automatic detection of the five classes in a single kymograph, displaying the level of confidence normalized to 1 for each category recognition.

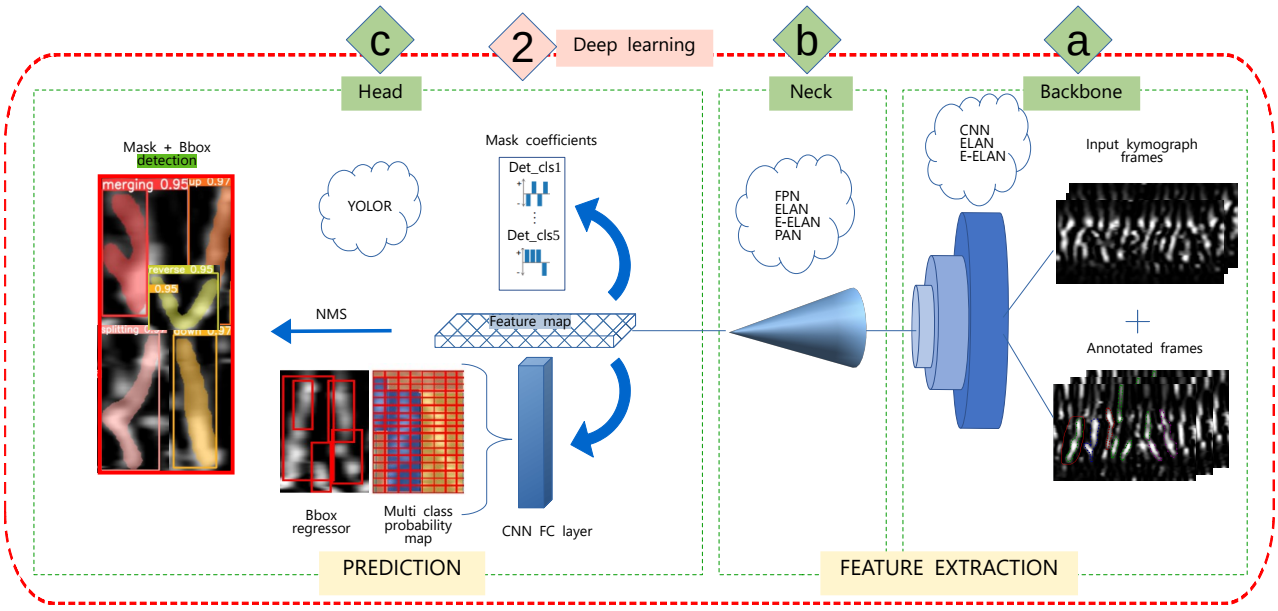

FIG. 8: Overview of the kymograph detection procedure using machine learning method. **(a)** Backbone module is responsible for feature extraction, **(b)** Neck module is used to fuse features from different levels of the backbone network to improve detection accuracy, **(c)** Head is responsible for predicting bounding boxes and class probabilities for each anchor. [color online]

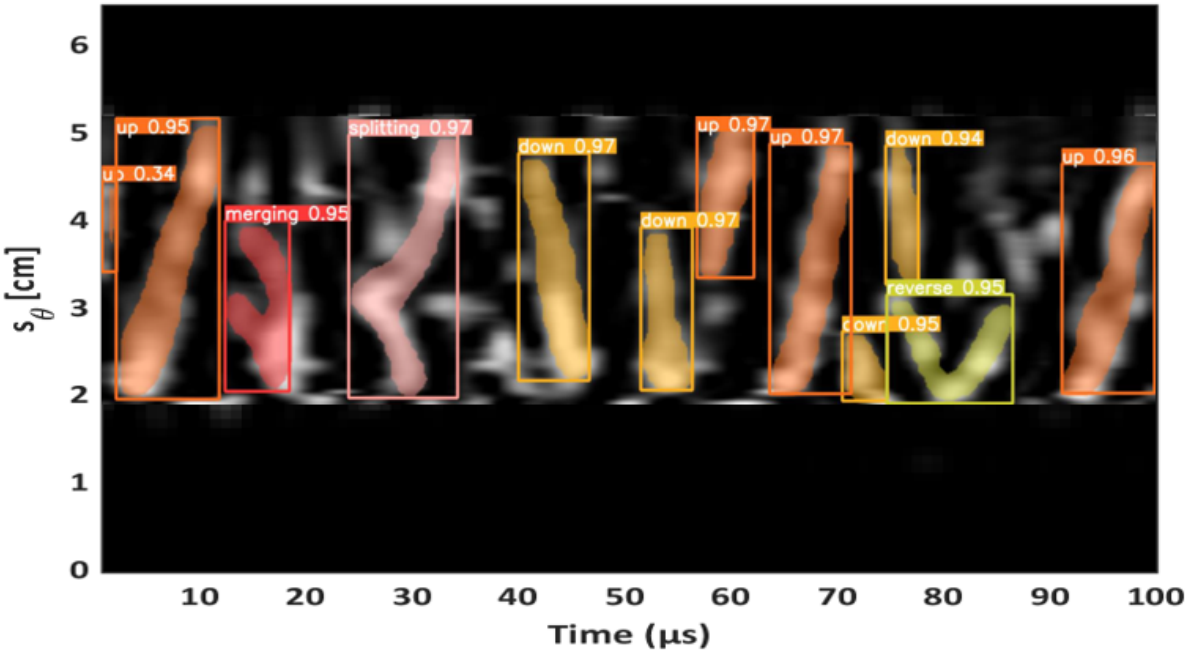

FIG. 9: Kymograph depicting the five detected classes with the ML method. The numbers refer to the model level of certainty, normalized to 1. [color online]

Appendix B: Blobs radial motion dynamics

In addition to the dynamics of the blobs in the poloidal direction, conventional tracking techniques can be used to characterize their radial motion. The 2D map of the temporally averaged radial velocities for shot #20846 is depicted in Fig. 10.

In a similar way to poloidal dynamics, the time-averaged radial flow does not account for the complexity of the individual radial movement of the blobs. The time-averaged probability density functions (PDFs) of radial velocities in a 4 mm square are depicted in Fig. 11(a), as well as the time series of radial velocities in the same zone (Fig. 11(b)). This figure demonstrates that there exist counter-propagating blobs and fast reversal of the blob motion also in the radial direction.

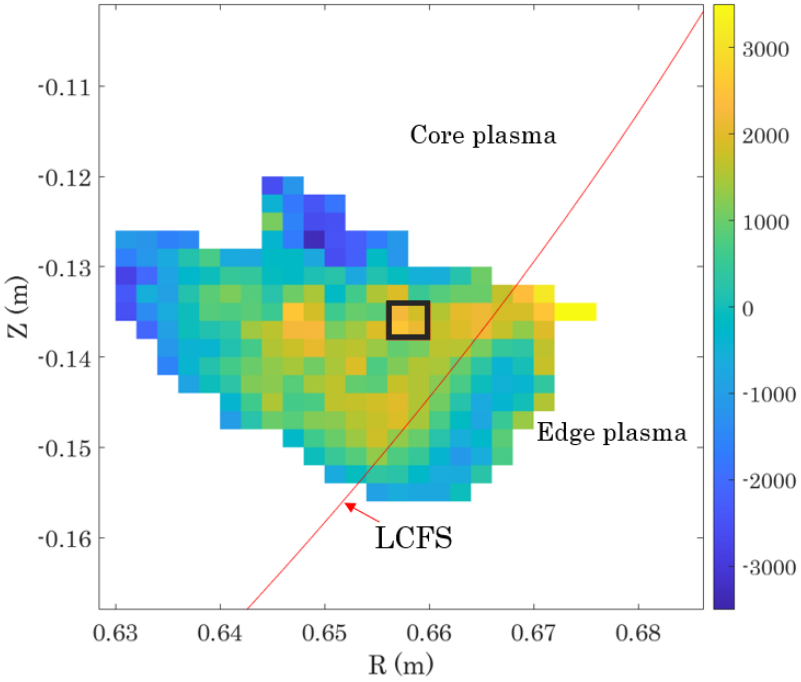

FIG. 10: 2D map of the mean radial velocities per pixel (m/s) of shot 20846 at [1100 - 1146.6]ms; the black square is the selected area used in Fig.11. [color online]

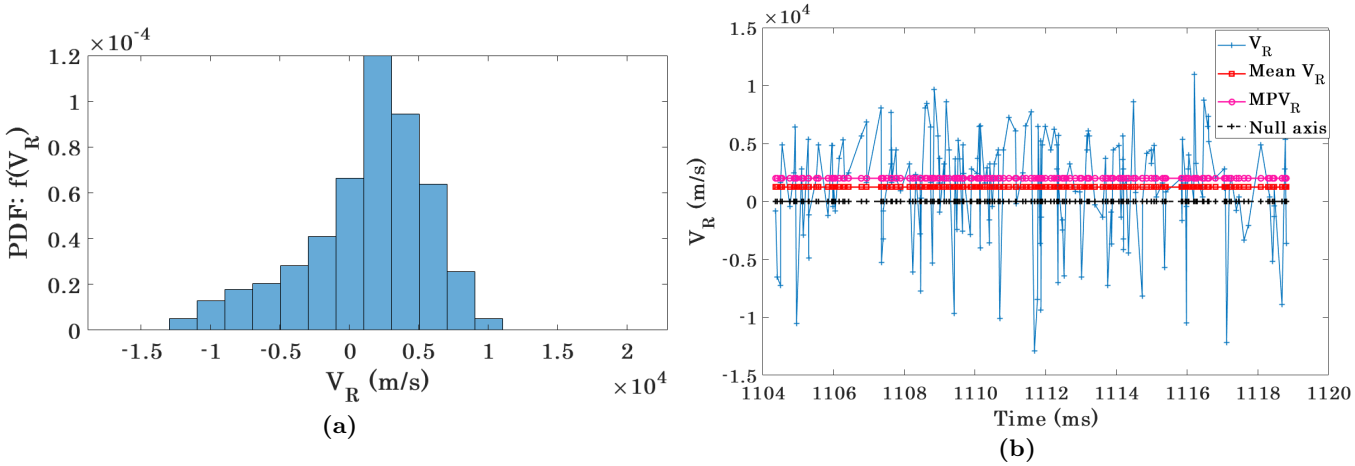

FIG. 11: (a), PDF of the radial velocities of filaments in the area included in the black square depicted in Fig. 10, where the most probable velocity $MPV = 2000$ m/s and the Mean $V_R = 1235$ m/s; (b) temporal variations of radial velocities, inside the selected area. In the captions, R is for radial velocity. [color online]

[1] *U.S. Innovation to meet 2050 climate goals*, Report (The White House, The White House, Washington, 2022).

[2] J. Achenbach and E. Halper, *U.S. announces milestone on fusion energy, sparking hopes for clean power*, Report (The Washington post, 2022).

[3] J. Tollefson and E. Gibney, Nuclear-fusion lab achieves 'ignition': what does it mean?, Nature **612 7941**, 597 (2022).

[4] D. Chandler, Mit-designed project achieves major advance toward fusion energy, e-print MIT News (2021).

[5] G. Harrer, M. Faitsch, L. Radovanovic, E. Wolfrum, C. Albert, A. Cathey, M. Cavedon, M. Dunne, T. Eich, R. Fischer, M. Griener, M. Hoelzl, B. Labit, H. Meyer, F. Aumayr, T. A. U. Team, and T. E. M. Team, Quasicontinuous exhaust scenario for a fusion reactor: the renaissance of small edge localized modes, Physical Review Letters **129**, 165001 (2022).

[6] O. A. Hurricane, P. K. Patel, R. Betti, D. H. Froula, S. P. Regan, S. A. Slutz, M. R. Gomez, and M. A. Sweeney, Physics principles of inertial confinement fusion and u.s. program overview, Reviews of Modern Physics **95(2)**.

[7] ITER Website, `https://www.iter.org/`, accessed: April 2023.

[8] Fusion Industry Association annual reports, `https://www.fusionindustryassociation.org/about-fusion-industry/`, accessed: september 2023.

[9] A. Fasoli, Essay: Overcoming the obstacles to a magnetic fusion power plant., Physical review letters **130 22**, 220001 (2023).

[10] J. Ongena, R. Koch, R. Wolf, and H. Zohm, Magnetic-confinement fusion, Nature Physics **12**, 398 (2016).

[11] N. Katz, J. Egedal, W. Fox, A. Y. Le, and M. Porkolab, Experiments on the propagation of plasma filaments., Physical review letters **101 1**, 015003 (2008).

[12] C. Theiler, I. Furno, P. Ricci, A. Fasoli, B. Labit, S. Müller, and G. Plyushchev, Cross-field motion of plasma blobs in an open magnetic field line configuration, Physical Review Letters **103**, 065001 (2009).

[13] D. Carralero, P. Manz, L. Aho-Mantila, G. Birkenmeier, M. Brix, M. Groth, H. Müller, U. Stroth, N. Vianello, E. Wolfrum, A. U. team, J. Contributors, and E. M. Team, Experimental validation of a filament transport model in turbulent magnetized plasmas, Physical Review Letters **115**, 215002 (2015).

[14] H. D. Sterck, S. Poedts, and J. P. Goedbloed, Dynamics of hot filaments in a tokamak plasma, Journal of Plasma Physics **59**, 277 (1998).

[15] W. Han, R. Pietersen, R. Villamor-Lora, M. Beveridge, N. Offeddu, T. Golfinopoulos, C. Theiler, J. L. Terry, E. Marmar, and I. Drori, Tracking blobs in the turbulent edge plasma of a tokamak fusion device, Scientific Reports **12.1**, 18142 (2021).

[16] S. J. Zweben, J. L. Terry, D. P. Stotler, and R. J. Maqueda, Invited review article: Gas puff imaging diagnostics of edge plasma turbulence in magnetic fusion devices., The Review of scientific instruments **88 4**, 041101 (2017).

[17] S. J. Zweben, J. A. Boedo, O. Grulke, C. Hidalgo, B. LaBombard, R. J. Maqueda, P. Scarin, and J. L. Terry, Edge turbulence measurements in toroidal fusion devices, Plasma Physics and Controlled Fusion **49.7**, S1.S23 (2007).

[18] J. L. Terry, S. J. Zweben, K. Hallatschek, B. LaBombard, R. J. Maqueda, B. Bai, C. J. Boswell, M. Greenwald, D. Kopon, W. M. Nevins, C. S. Pitcher, B. N. Rogers, D. P. Stotler, and X. Q. Xu, Observations of the turbulence in the scrape-off-layer of alcator c-mod and comparisons with simulation, Physics of Plasmas **10**, 1739 (2003).

[19] R. Maqueda, G. Wurden, D. Stotler, S. Zweben, B. LaBombard, J. L. Terry, J. Lowrance, V. Mastrocola, G. Renda, D. D'Ippolito, J. Myra, and N. Nishino, Gas puff imaging of edge turbulence, Review of scientific instruments **74 3**, 2003 (2003).

[20] S. Zweben, D. Stotler, J. L. Terry, B. LaBombard, M. Greenwald, M. Muterspaugh, C. S. Pitcher, A. C.-M. Group, K. Hallatschek, R. J. Maqueda, B. Rogers, J. L. Lowrance, V. J. Mastrocola, and G. F. Renda, Edge turbulence imaging in the alcator c-mod tokamak, Phys. Plasmas **9 5**, 1981 (2002).

[21] I. Cziegler, J. L. Terry, J. Hughes, and B. LaBombard, Experimental studies of edge turbulence and confinement in alcator c-mod, Physics of Plasmas **17**, 056120 (2010).

[22] . M. Hron et al, Overview of the compass results, Nuclear Fusion **62**, 042021 (2021).

[23] R. N. van yen, N. Fedorczak, F. Brochard, G. Bonhomme, K. Schneider, M. Farge, and P. Monier-Garbet, Tomographic reconstruction of tokamak plasma light emission from single image using wavelet-vaguelette decomposition, Nuclear Fusion **52**, 013005 (2011).

[24] J. Cavalier, N. Lemoine, F. Brochard, V. Weinzettl, J. Seidl, S. A. Silburn, P. Tamain, R. Dejarnac, J. Adamek, and R. Pánek, Tomographic reconstruction of tokamak edge turbulence from single visible camera data and automatic turbulence structure tracking, Nuclear Fusion **59.5**, 056025 (2019).

[25] F. Militello, B. D. Dudson, L. Easy, A. Kirk, and P. W. Naylor, On the interaction of scrape off layer filaments, Plasma Physics and Controlled Fusion **59**, 125013 (2017).

[26] F. Nespoli, P. Tamain, N. Fedorczak, G. Ciraolo, D. Galassi, R. Tatali, E. Serre, Y. Marandet, H. Bufferand, and P. Ghendrih, 3d structure and dynamics of filaments in turbulence simulations of west diverted plasmas, Nuclear Fusion **59**, 096006 (2019).

[27] O. E. Garcia, S. Fritzner, R. Kube, I. Cziegler, B. LaBombard, and J. L. Terry, Intermittent fluctuations in the alcator c-mod scrape-off layer, Physics of Plasmas **20**, 055901 (2012).

[28] N. R. Walkden, A. Wynn, F. Militello, B. Lipschultz, G. F. Matthews, C. Guillemaut, J. R. Harrison, and D. Moulton, Statistical analysis of the ion flux to the jet outer wall, Nuclear Fusion **57.3**, 036016 (2016).

[29] J. P. Lynov, P. K. Michelsen, H. L. Pécseli, and J. J. Rasmussen, Interaction between electron holes in a strongly magnetized plasma, Physics Letters A **80**, 23 (1980).

[30] S. Zweben, J. Myra, W. Davis, D. D'Ippolito, T. Gray, S. Kaye, B. LeBlanc, R. Maqueda, D. Russell, D. Stotler, and the NSTX-U Team, Blob structure and motion in the edge and sol of nstx, Plasma Physics and Controlled Fusion **58**, 044007 (2016).

[31] M. Lampert, A. Diallo, J. Myra, and S. Zweben, Dynamics of filaments during the edge-localized mode crash on

nstx, Physics of Plasmas **28**, 022304 (2021).

[32] N. Offeddu, C. Wüthrich, W. Han, C. Theiler, T. Golfinopoulos, J. L. Terry, E. Marmar, A. Ravetta, and G. V. Parys, Analysis techniques for blob properties from gas puff imaging data, Review of scientific instruments **94 3**, 033512 (2023).

[33] C. Wüthrich, C. Theiler, N. Offeddu, D. Galassi, D. S. Oliveira, B. Duval, O. Février, T. Golfinopoulos, W. Han, E. Marmar, J. L. Terry, C. K.-W. Tsui, and the TCV team, X-point and divertor filament dynamics from gas puff imaging on tcv, Nuclear Fusion **62** (2022).

[34] Y. Wu, Y. Zhu, G. Bai, Y. Wang, and G. Chiribella, Quantum similarity testing with convolutional neural networks., Physical review letters **130 21**, 210601 (2022).

[35] A. Boehnlein, M. Diefenthaler, N. Sato, M. Schram, V. Ziegler, C. Fanelli, M. Hjorth-Jensen, T. Horn, M. P. Kuchera, D. Lee, W. Nazarewicz, P. N. Ostroumov, K. Orginos, A. Poon, X.-N. Wang, A. Scheinker, M. S. Smith, and L. Pang, Colloquium: Machine learning in nuclear physics, Reviews of Modern Physics **94**, 031003 (2021).

[36] J. H. wen Hsiao, J. An, V. K. S. Hui, Y. Zheng, and A. B. Chan, Understanding the role of eye movement consistency in face recognition and autism through integrating deep neural networks and hidden markov models, NPJ Science of Learning **7.1**, 28 (2022).

[37] A. A. Shah, H. A. M. Malik, A. H. Muhammad, A. Alourani, and Z. A. Butt, Deep learning ensemble 2d cnn approach towards the detection of lung cancer, Scientific Reports **13.1**, 2987 (2023).

[38] X. Cheng, S. Zhang, P. C. H. Nguyen, S. Azarfar, G.-W. Chern, and S. Baek, Convolutional neural networks for large-scale dynamical modeling of itinerant magnets, Physical Review Research **2306.11833** (2023).

[39] E. V. Miu, J. R. McKone, and G. Mpourmpakis, Global and local connectivities describe hydrogen intercalation in metal oxides, Physical Review Letters **131**, 108001 (2023).

[40] C.-Y. Wang, A. Bochkovskiy, and H.-Y. M. Liao, Yolov7: Trainable bag-of-freebies sets new state-of-the-art for real-time object detectors, 2023 IEEE/CVF Conference on Computer Vision and Pattern Recognition (CVPR) , 7464 (2022).

[41] A. Mathews, M. Francisquez, J. W. Hughes, D. R. Hatch, B. Zhu, and B. N. Rogers, Uncovering turbulent plasma dynamics via deep learning from partial observations., Physical review. E **104 2-2**, 025205 (2020).

[42] A. Mathews, J. Hughes, J. L. Terry, and S. G. Baek, Deep electric field predictions by drift-reduced braginskii theory with plasma-neutral interactions based upon experimental images of boundary turbulence, Physical review letters **129 23**, 235002 (2022).

[43] APREX Solutions website, `https://aprex-solutions.com/en/`, accessed: september 2023.

[44] K. Jiráková, O. Kovanda, J. Adamek, M. Komm, and J. Seidl, Systematic errors in tokamak magnetic equilibrium reconstruction: a study of efit++ at tokamak compass, Journal of Instrumentation **14**, C11020.

[45] S. Zweben, W. Davis, S. Kaye, J. Myra2, R. Bell, B. LeBlanc, R. Maqueda, T. Munsat, S. Sabbagh, Y. Sechrest, D. Stotler, and the NSTX Team, Edge and sol turbulence and blob variations over a large database in nstx, Nucl. Fusion **55 9**, 093035 (2015).

[46] T. Farley, N. Walkden, F. Militello, M. Sanna, J. Young, S. S. Silburn, J. Harrison, L. A. Kogan, I. Lupelli, S. S. Henderson, A. Kirk, and J. W. Bradley, Filament identification in wide-angle high speed imaging of the mega amp spherical tokamak., The Review of scientific instruments **90 9**, 093502 (2019).

[47] S. Silburn, J. Harrison, T. Farley, J. Cavalier, S. V. Stroud, J. McGowan, A. Marignier, E. Nurse, C. Gutschow, M. Smithies, A. Wynn, and R. Doyle, Calcam (2023).

[48] M. Mikikian, H. Tawidian, and T. Lecas, Merging and splitting of plasma spheroids in a dusty plasma., Physical review letters **109 24**, 245007 (2012).

[49] C.-Y. Wang, H. Liao, and I.-H. Yeh, Designing network design strategies through gradient path analysis, ArXiv **abs/2211.04800** (2022).

[50] Z. Cao, R. Li, X. Yang, L. Fang, Z. Li, and J. Li, Multiscale detection of pulmonary nodules by integrating attention mechanism, Scientific Reports **13.1**, 5517 (2023).

[51] T.-Y. Lin, P. Dollár, R. B. Girshick, K. He, B. Hariharan, and S. J. Belongie, Feature pyramid networks for object detection, 2017 IEEE Conference on Computer Vision and Pattern Recognition (CVPR) , 2117 2125 (2016).

[52] S. Liu, L. Qi, H. Qin, J. Shi, and J. Jia, Path aggregation network for instance segmentation, 2018 IEEE/CVF Conference on Computer Vision and Pattern Recognition , 8759 8768 (2018).

[53] C.-Y. Wang, I.-H. Yeh, and H. Liao, You only learn one representation: Unified network for multiple tasks, J. Inf. Sci. Eng. **39**, 691 (2021).

[54] A. Neubeck and L. V. Gool, Efficient non-maximum suppression, 18th International Conference on Pattern Recognition (ICPR'06) **3**, 850 (2006).